Fusion Engineering and Design 214 (2025) 114903

Contents lists available at ScienceDirect

Fusion Engineering and Design

journal homepage: www.elsevier.com/locate/fusengdes

Thermofluid-dynamic assessment of the dual cooling scheme EU-DEMO divertor cassette

F.M. Castrovinci [a], A. Quartararo [a,*], S. Basile [a], G. Bongiovì [a], R. Burlon [a], P. Chiovaro [a], P.A. Di Maio [a], A. Gioè [a], S. Maggio [a], G. Mazzone [c], E. Tomarchio [a], S. Vacca [a], E. Vallone [a], J.-H. You [b]

[a] Department of Engineering, University of Palermo, Viale delle Scienze Ed. 6, 90128, Palermo, Italy
[b] Max Planck Institute of Plasma Physics (E2M), Boltzmann Str.2, 85748, Garching, Germany
[c] Department of Fusion and Technology for Nuclear Safety and Security, ENEA C. R. Frascati, via E. Fermi 45, 00044, Frascati (Roma), Italy

ARTICLE INFO

Keywords:
DEMO
Divertor
CFD analysis
Thermofluid-dynamics

ABSTRACT

The EU-DEMO divertor is currently foreseen to employ a dual cooling scheme, which involves two separate cooling circuits for the Cassette Body (CB) and the Vertical Targets (VTs), provided with cooling water at distinct operating conditions. Following the EU-DEMO project Gate Review 1, the cassette design has been revised to employ a high-temperature (295-328 °C) and high-pressure (15.5 MPa) coolant for the CB cooling circuit. These design assumptions present novel challenges in achieving uniform and effective cooling of the structure, to ensure reliable operation over the intended lifetime. Furthermore, alternative materials for the VTs-supporting Target Support Bodies (TSBs), namely CuCrZr, SS 316Ti and Eurofer97, are currently being evaluated to extend the operational lifetime of these components under irradiation. The University of Palermo, in collaboration with EUROfusion and ENEA, analysed the steady-state thermal-hydraulic performance of the EU-DEMO divertor cooling circuits with an integrated conjugate heat transfer analysis campaign of the entire divertor cassette, with the twofold aim to evaluate the CB thermal performance under the revised coolant conditions and to compare the temperature distribution in the TSBs with the different materials considered. The work was carried out following a numerical approach based on the finite volume method and adopting the ANSYS CFX computational fluid-dynamic commercial code. Models, loads and boundary conditions are herewith reported and critically discussed, together with the main outcomes obtained.

1. Introduction

The divertor is a crucial in-vessel component in future nuclear fusion power plants, being responsible for several essential functions that enable stable and long-pulse reactor operation. It must withstand the intense power deposited by charged particles and neutron irradiation, facilitate the removal of fusion ashes and unburnt fuel towards the pumping ports, provide plasma-facing surfaces compatible with the plasma, and shield both the Vacuum Vessel (VV) and surrounding magnets from nuclear loads [1].

The divertor cooling circuit has to be designed to manage the large heat and particle fluxes coming from the plasma, to ensure that the structural and functional materials operate within their temperature limits (to enhance the component lifetime and thus reduce the nuclear waste), to guarantee limited pressure losses, and to operate at high temperatures to maximise the plant electricity conversion efficiency.

The European Demonstration Power Plant (EU-DEMO) divertor currently employs a dual cooling scheme [1], which provides cooling water at distinct operating conditions to the Vertical Targets (VTs) and to the Cassette Body (CB), depending on their thermal requirements.

The selection of coolant operating conditions for the DEMO divertor has been a debated topic in recent years. While past research activities considered a low-temperature coolant for the CB cooling circuit, devoted to providing coolant to the Eurofer97 components [2,3], recently the possibility of employing a high pressure and temperature coolant has been investigated to extend the operational lifetime under irradiation of these components [4]. For the same reason, different materials are currently under investigation for the low-temperature VTs structural components.

In 2023, as part of the activities promoted by the EUROfusion Work Package Divertor, a research campaign was jointly carried out

* Corresponding author.
E-mail address: andrea.quartararo@unipa.it (A. Quartararo).

https://doi.org/10.1016/j.fusengdes.2025.114903
Received 6 December 2024; Received in revised form 30 January 2025; Accepted 24 February 2025
Available online 5 March 2025

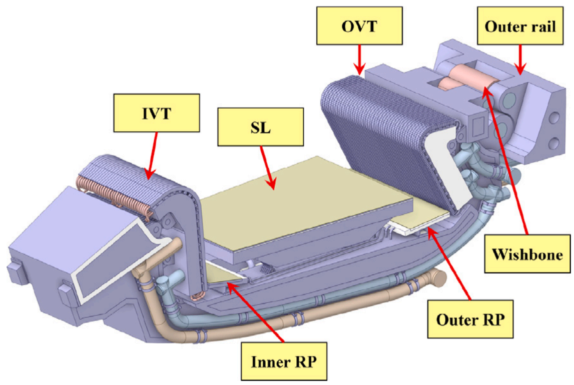

Fig. 1. EU-DEMO divertor cassette (High-pressure, dual-cooling circuit option).

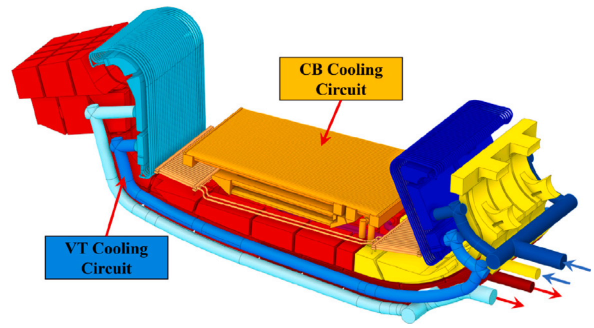

Fig. 2. Divertor cassette (High pressure, dual-cooling circuit option) cooling circuits.

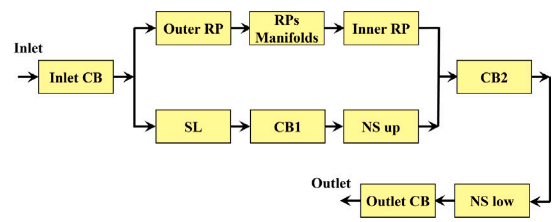

Fig. 3. Divertor CB cooling circuit flow routing.

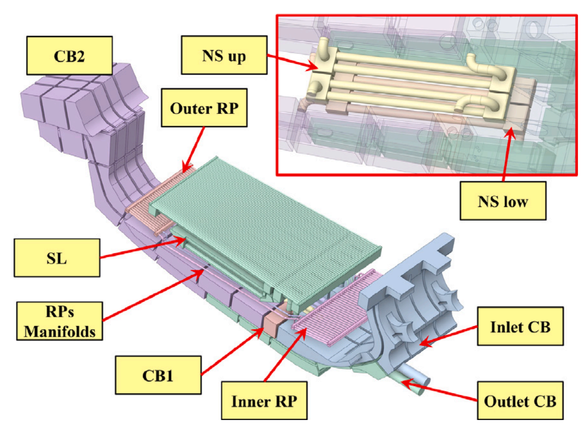

Fig. 4. Divertor CB cooling circuit region nomenclature.

between the University of Palermo and ENEA to assess the steady-state thermal-hydraulic performance of the EU-DEMO divertor cooling circuits with the CB operated at high-temperature and high-pressure, while considering different structural materials for the VTs Target Support Bodies (TSBs).

The research campaign was conducted with a numerical approach based on the finite volume method and adopting the ANSYS CFX 2021 R1 Computational Fluid-Dynamic (CFD) code [5].

2. General description of the high-pressure dual cooling scheme DEMO divertor cassette

The EU-DEMO divertor currently consists of 48 toroidal cassette modules. Each module comprises a CB supporting the components directly exposed to the plasma, i.e. a Shielding Liner (SL), two Reflector Plates (RPs), and two VTs, namely an Outer VT (OVT) and an Inner VT (IVT). Each cassette is moreover equipped with a couple of Neutron Shields (NSs). The cassette fixation system to the VV relies on two noses at the inboard, while at the outboard it is foreseen the adoption of a wishbone. It is designed to provide the flexibility needed to accommodate differential thermal expansion of the VV and cassette, while maintaining the divertor's position and mitigating shaking motion during vertical displacement events, cold disruptions, and other dynamic plasma scenarios. The wishbone is locked to an outer rail, mechanically connected to the VV.

The EU-DEMO high-pressure, dual-cooling circuit option cassette design [6] is shown in Fig. 1 with an indication of the main components (the NSs are not visible, being inside the vacuum pumping hole).

The EU-DEMO divertor is water-cooled, and the two cooling circuits adopted are depicted in Fig. 2. The design driver for the VTs cooling circuit is the necessity to withstand nominal peak heat fluxes up to 20 MW/m^2 [1] without incurring into Critical Heat Flux (CHF) issues, thus requiring outstanding cooling performances. Instead, the CB cooling circuit is characterised by lower thermal loads, thus allowing a greater degree of freedom to explore different coolant operating conditions, potentially optimising component lifetime and plant integration.

As it may be argued from Fig. 2, the two VTs are connected in series to each other, and the coolant routing is made possible by a set of connecting pipes running along the sides of the cassette. The adoption of VTs in series allows for a lower coolant mass flow rate, but the requirement to maintain the CuCrZr Plasma Facing Units (PFUs) assemblies cooling pipes at temperatures not lower than 130 °C (to avoid a further decrease from the minimum thermal recovery temperature of irradiated CuCrZr of 150 °C [1]) requires a higher coolant inlet pressure of ≈7.5 MPa [4], compared to the 5.0 MPa employed with the VTs connected in parallel [7].

The PFUs assemblies, whose details can be found in [1], are mounted on dedicated TSBs. Different materials are under investigation for the TSBs and, in this paper, the effects of the selection of either CuCrZr, SS 316 Ti, and Eurofer97 on the cooling performance of the divertor are investigated.

Concerning the CB cooling circuit, its layout is rather complex, as shown in Fig. 3 with the region nomenclature depicted in Fig. 4.

The details of the cooling layout of the singular divertor components are unchanged compared to the previous divertor designs and can be found in [8]. The main differences are the coolant routing inside the CB and the NSs cooling layout. This latter has been redesigned to a simpler solution with four cooling channels moving along the radial direction for each NS, as visible in Fig. 4.

According to the rationale described in [4], the CB cooling circuit is fed with cooling water at Pressurized Water Reactor (PWR)-like conditions, i.e. at an inlet pressure of 15.5 MPa and an inlet temperature of 295 °C, to reduce the risk of operating the irradiated Eurofer97 in brittle conditions [9]. Moreover, as the same coolant operating conditions are considered for the Water-Cooled Lead Lithium Breeding Blanket [10], plant integration could be potentially simplified [11].

The revised CB coolant operating conditions present novel challenges in achieving uniform and effective cooling of the structure, as will be discussed in the following.

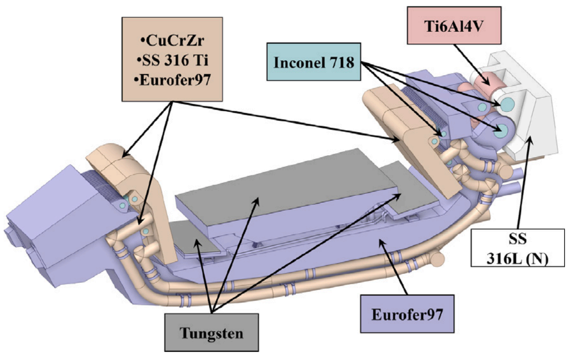

Fig. 5. Structure domains considered for the CHT analyses and details of the different materials.

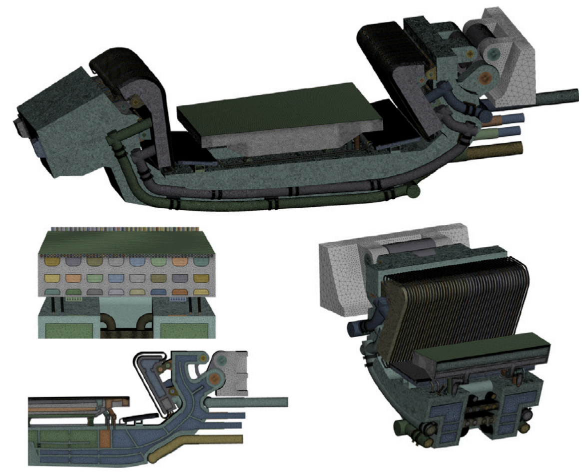

Fig. 6. Mesh adopted for the thermofluid-dynamic CHT analysis.

3. Divertor cooling circuit CFD analysis setup

The thermofluid-dynamic assessment of the divertor cassette was performed by running 3D steady-state Conjugate Heat Transfer (CHT) analyses. With respect to past years' investigations on dual cooling scheme divertor designs [3,7], the study was approached with integrated simulations encompassing both cooling circuits, as the TSBs supports have proven to be particularly critical in terms of thermal hot spots [8].

All the divertor cassette geometrical details have been included in the simulations, except for the PFU assemblies. For these components, the structures are not modelled, while the effects of the swirl tapes on the coolant flow are treated with the Orthotropic Virtual Swirl Tape (OVST) approach [12] to ensure an acceptable computational burden without significantly affecting the results accuracy.

Additionally, compared to past simulations, the cassette CHT model was further advanced by inserting the outer rail (depicted in Fig. 1) to improve the temperature predictions on the wishbone, and by including further elements of the TSBs supports, detailing the different materials of hinges and pins.

The structure domains considered in the CHT analyses are depicted in Fig. 5, with an indication of the different materials (each colour corresponds to a different material). Three distinct simulations were performed, one for each material considered for the TSBs and their feeding pipes.

The computational grid employed for the calculations was defined by selecting suitable features, based on past mesh-independence studies [8]. The mesh details are visible in Fig. 6, while the main parameters and quality metrics are summarised in Table 1. The large mesh size necessitated the use of the computational resources provided by the CRESCO/ENEAGRID High Performance Computing infrastructure [13].

To perform the simulations, the coolant operating conditions summarised in Table 2 were considered. Concerning the VTs cooling circuit, a coolant mass flow rate (G) of 45 kg/s was selected based on preliminary parametric analyses performed with the code ADRANOS [14], as reported in [4].

Regarding the CB cooling circuit, instead, a mass flow rate of ≈17 kg/s was chosen to provide the desired coolant outlet-inlet temperature increase ΔT of 33 °C for each simulation.

Surface heat loads on SL, RPs, and VTs were drawn from [15] while the nuclear contributions were provided by the ENEA Frascati Neutronics Team for the high-pressure divertor design and dedicated neutronic simulation results are available for each material selected for the TSBs and their connection pipes [16]. The nuclear load breakdown is summarised for different cases in Table 3.

As one may argue from the table, the thermal loads have high variations for the VTs cooling circuit due to the different materials employed, and the higher values are foreseen for the case with TSBs in CuCrZr. There are some variations in the CB nuclear loads as well, but the differences among the three cases are smaller.

Table 1
Summary of the main mesh parameters and quality metrics.

Region	Mesh parameter	Value
Coolant	Mesh Type	Hybrid
	Nodes	$9.05 \cdot 10^7$
	Elements	$1.31 \cdot 10^8$
	Inflation Layers Number	12
	First Cell Height [μm]	20 – 50
	Layers Growth Rate	1.2 – 1.35
	Target Element Size [mm]	1.3 – 10
	Surface with y^+>200 [%]	0.02
Structure	Mesh Type	Hybrid
	Nodes	$2.03 \cdot 10^7$
	Elements	$9.29 \cdot 10^7$
	Target Element Size [mm]	2.5 – 10
Quality	Orthogonal Angle [°] (ave/min)	76.3/0.34
	Expansion Factor (ave/max)	1.85/11980
	Aspect Ratio (ave/max)	29/1809

Table 2
Summary of coolant operative conditions for the two cooling circuits.

	VTs Cooling Circuit	CB Cooling Circuit
Coolant p_{in} [MPa]	7.5	15.5
Coolant T_{in} [° C]	130	295
G per cassette [kg/s]	45	≈17
Total Deposited Power [MW]	3.7-4.0	≈3.4
Coolant ΔT [° C]	≈22	33

Table 3
Nuclear heating breakdown for the three different TSBs materials [MW].

	CuCrZr	SS 316 Ti	Eurofer97
OVT	0.770	0.611	0.623
IVT	0.783	0.608	0.618
Pipes	0.034	0.028	0.030
Total VTs	1.587	1.247	1.272
CB	0.808	0.785	0.784
SL	1.639	1.635	1.651
RPs	0.328	0.326	0.322
Total CB	2.775	2.746	2.757

4. Divertor cooling circuit CFD analysis results

The steady-state thermal-hydraulic performances of the divertor cooling circuits under the operative conditions of Table 2 were assessed to check whether the compliance with the applicable constraints [14, 17] is met:

Table 4
Summary of assumptions, models and BCs.

Analysis type	Steady-state CHT
Material Library	Water IAPWS IF97 [20] Eurofer97 [21] W, Ti6Al4V [22] SS 316 Ti, Inconel 716 [23] CuCrZr [24] SS 316L (N) [25]
Liner/RPs Heat Flux	From [15]
Nuclear Heating	From [16]
Radiative Heat Transfer	Towards VV @ 40 °C [26]
Turbulence Model	k-ω SST
Boundary Layer Modelling	Automatic Wall Functions
PFU Assembly Modelling	OVST
Wall Roughness	15 μm
Wall Roughness PFUs	2 μm
Inlet BC - VTs	T=130 °C/p_{tot}=7.5 MPa
Outlet BC - VTs	G=45 kg/s
Inlet BC - CB	T=295 °C/p_{tot}=15.5 MPa
Outlet BC - CB	G adjusted for ΔT=33 °C

Fig. 7. VT cooling circuit absolute pressure field distribution.

- maximum temperature in Eurofer97 < 550 °C;
- total pressure drop for each cooling circuit < 1.4 MPa;
- coolant local minimum saturation margin > 20 °C;
- coolant maximum axial velocity in PFUs cooling channels < 16 m/s;
- minimum CHF margin.[1] > 1.4 in PFUs, SL and RPs cooling channels under nominal heat flux conditions.

The three simulations were performed considering the assumptions, models and Boundary Conditions (BCs) summarised in Table 4. The guidelines of [19] were followed to ensure the quality of the results obtained and each CHT simulation required ≈24 h of calculation time to perform 2000 iterations on the ENEA CRESCO cluster, running on 672 Intel Xeon Platinum 8160 processors @2.10 GHz.

The results obtained in terms of pressure drop, coolant distributions, CHF and saturation margins are reported only for the case with TSBs in CuCrZr, as the results are practically the same for the three cases considered. In fact, the mass flow rate in the CB cooling circuit changes by less than 1% due to the different nuclear heat loads of Table 3, while the VTs cooling circuit mass flow rate is the same for all the simulations, as it is only defined by CHF margin requirements. Therefore, the only differences are related to the small variations in coolant density with temperature which are very limited as the VTs cooling circuit outlet temperature is ≈149.5 °C for the Eurofer97 and SS 316 Ti cases and ≈151.4 °C for the CuCrZr simulation.

The pressure distribution in the VTs and CB cooling circuit is depicted respectively in Figs. 7 and 8, while the total pressure drop of the two cooling circuits amounts to 1.13 and 0.50 MPa, lower than the limit value of 1.40 MPa.

[1] The definition of CHF margin can be found in [18]

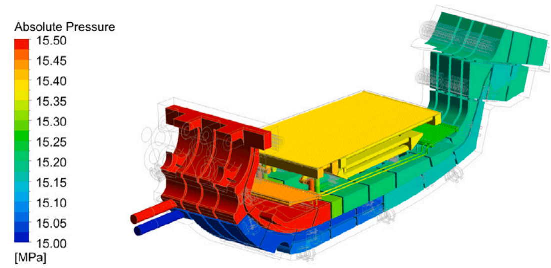

Fig. 8. CB cooling circuit absolute pressure field distribution.

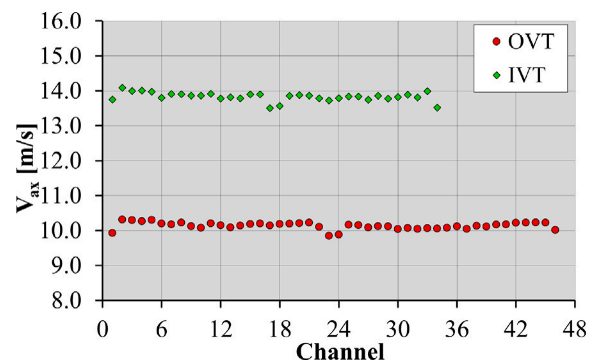

Fig. 9. Coolant axial flow velocity distribution among PFU channels.

It is moreover worth mentioning that the pressure drop in the VTs cooling circuit is mainly due to the IVT, contributing alone for more than 50% of the total losses, while the SL and RPs present the highest pressure losses in the CB cooling circuit.

About the pressure drop limit of the CB cooling circuit, it should be observed that the 1.4 MPa value was originally selected for a cassette operating at 180 °C inlet temperature and 3.5 MPa inlet pressure [17]. The adoption of a higher temperature mandates a revision of this limit, to compensate for the lower water density. In this regard, 0.7 MPa was already proposed in [4]. Even with this revised value, the pressure drop calculated for the EU-DEMO divertor CB cooling circuit is within the limits.

Concerning the coolant distribution, it is reported for the PFUs (Fig. 9), and for the SL (Fig. 10) and RPs (Fig. 11) cooling channels closest to the plasma.

As it may be argued from the figures, the coolant distribution is acceptably uniform for the PFUs and SL channels, while the RPs present a non-uniform distribution, with flow reversal in some channels.

Moreover, the coolant axial velocities in the PFUs cooling channels are ≈14 m/s. Despite it would be beneficial to lower these velocities to lower values to avoid potential swirl tape fretting issues, it was prioritised to operate the CuCrZr at suitable temperatures, as is not possible to reduce the VTs cooling circuit mass flow rates without decreasing the inlet temperature below 130 °C [4].

The margins against CHF were calculated at the post-processing stage by adopting the same procedure discussed in [8], i.e. the modified Tong-75 correlation [18] was employed for the PFU cooling channels and the Groeneveld look-up tables [27] for SL and RPs. The calculations were performed considering nominal heat flux values for these components, i.e. 20 MW/m^2 for the PFUs, 1 MW/m^2 for the SL, and 0.2 MW/m^2 for the RPs. The results obtained are reported in the following Figs. 12 to 14 showing the minimum value of 1.4 with a dashed red line.

Acceptable CHF margins are calculated for the PFUs and the SL, while some RP channels present a zero margin, as visible in Fig. 14. This result can be explained by the presence of stagnant coolant in these

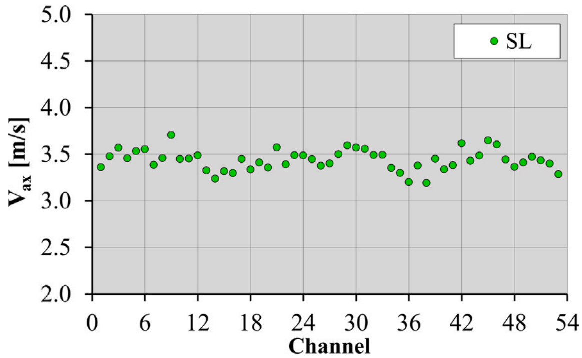

Fig. 10. Coolant axial flow velocity distribution among SL channels.

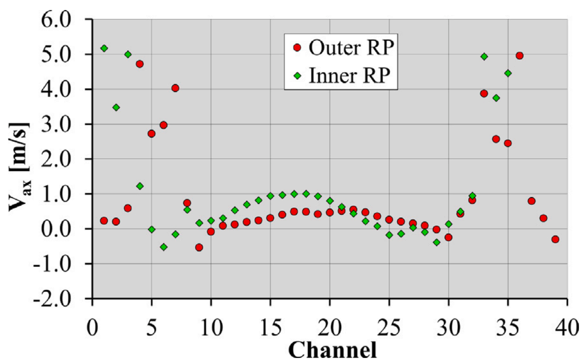

Fig. 11. Coolant axial flow velocity distribution among RPs channels.

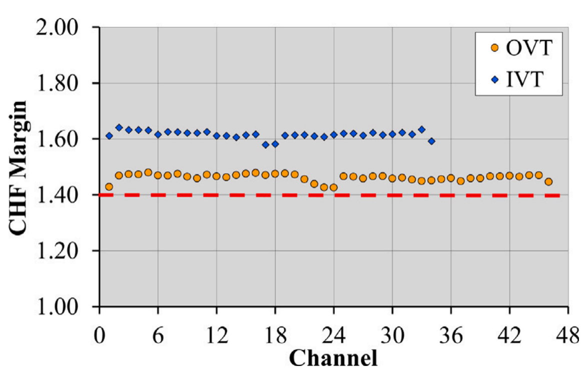

Fig. 12. CHF margin distribution among PFUs channels.

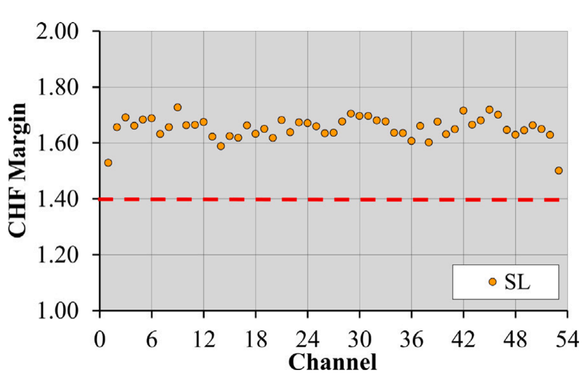

Fig. 13. CHF margin distribution among SL channels.

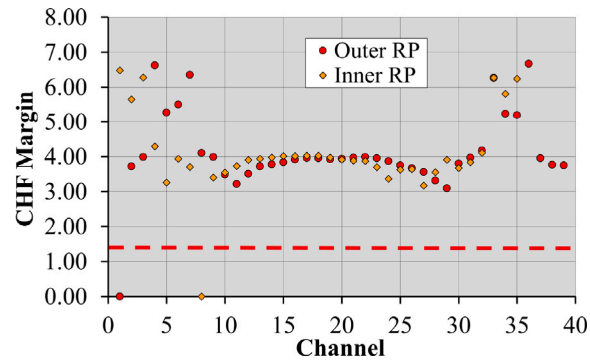

Fig. 14. CHF margin distribution among RPs channels.

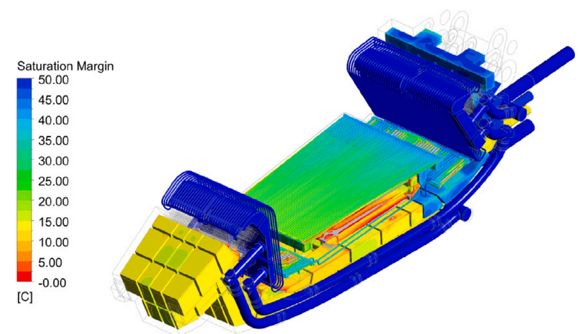

Fig. 15. Divertor coolant margin against saturation field.

channels, causing the fluid bulk temperature to overcome saturation. It can be confirmed by looking at the saturation margin field, depicted in Fig. 15, showing in grey the areas where the saturation margin is lower than zero: as it may be observed, some RP channels present vast critical areas.

It may be moreover observed from Fig. 15 how the entire VTs cooling circuit presents a high saturation margin, due to its high coolant pressure and low temperature, while the CB cooling circuit is characterised by various regions where the saturation margin is low or even below zero, suggesting the necessity of some design changes, e.g. in the SL and in some corners of the cassette.

Additionally, the coolant outlet bulk saturation margin is calculated to be 14 °C at the outlet of the CB cooling circuit, a value which is below the 20 °C requirement of [17]. In fact, the saturation margin limit was originally defined for a low-pressure and low-temperature cassette [3], and it is not applicable to the new operating conditions. Indeed, the water saturation temperature at 15.5 MPa is ≈345 °C [28] so, even supposing zero pressure drop inside the system, the saturation margin cannot be higher than 17 °C as a consequence of fixing the coolant outlet temperature to 328 °C.

Finally, as far as the structure temperature field is concerned, the temperatures obtained for the three different scenarios are reported in the following Figs. 16 to 18, respectively for the TSBs in CuCrZr, SS 316 Ti, and Eurofer97. The temperatures are shown from 130 °C to 550 °C, the latter being the maximum suggested temperature in Eurofer97. All the regions where the temperatures exceed this maximum value are shown in grey.

As one may observe, the major differences among the three cases are observed in the TSBs, both due to the different nuclear thermal loads and the distinct thermal conductivities of the materials. Although the highest thermal loads are expected for the CuCrZr case, as reported in Table 3, the thermal conductivity plays a stronger role. Therefore, the temperatures are the lowest for the CuCrZr case, while the highest values are obtained with SS 316 Ti, with values as high as 575 °C for

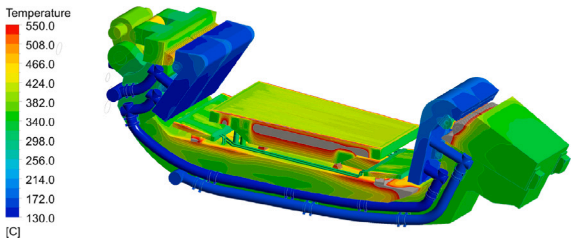

Fig. 16. Divertor structure temperature field with TSBs in CuCrZr.

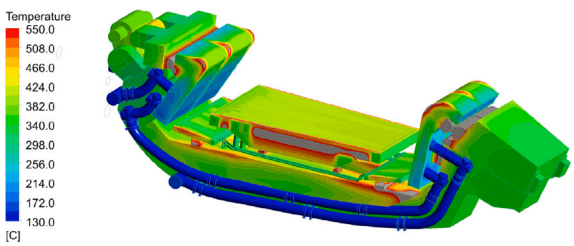

Fig. 17. Divertor structure temperature field with TSBs in SS 316 Ti.

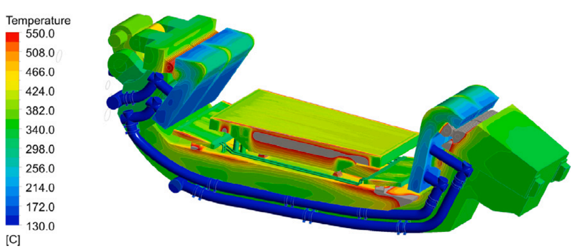

Fig. 18. Divertor structure temperature field with TSBs in Eurofer97.

the TSBs and even higher for their supports. Furthermore, there are common issues in all the cases, with Eurofer97 temperatures exceeding 550 °C in some regions of the CB, such as the SL side walls and some corners of the cassette, requiring the review of their cooling circuits. Indeed, high temperatures could pose problems in terms of fulfilment of the criteria prescribed by the reference structural design code, jeopardising the integrity of the components.

The major criticalities are related to the non-actively cooled supports of the SL, RPs, and TSBs, which are of particular concern. Similar issues have been observed in past EU-DEMO divertor designs [3,8], and can be solved by acting both on the reduction of the length of these supports and by improving the shielding performance of the supported components, e.g. by increasing their thickness.

Furthermore, compared to previous analyses [8], the temperature in the wishbone is significantly reduced, due to the different modelling strategy that includes the outboard rail.

Finally, although not shown for the sake of brevity, no thermal criticalities are observed for the revised NSs due to the very low volumetric thermal loads experienced by these components.

5. Conclusions

The University of Palermo, in collaboration with EUROfusion and ENEA, carried out a research campaign focused on the thermofluid-dynamic assessment of the novel high-pressure and high-temperature EU-DEMO divertor cassette under steady-state operational conditions. The studies were performed with an integrated CFD simulation approach encompassing both the divertor cooling circuits, made possible by the use of the ENEA CRESCO High Performance Computing infrastructure.

The results obtained highlighted good thermal-hydraulic performance for the VTs cooling circuit, assessed in terms of pressure drop, maximum velocity in the PFU cooling channels, CHF and saturation margins, confirming the outcomes of the studies performed for the selection of VTs cooling circuit operating conditions of [4].

The CB cooling circuit operated at PWR-like conditions presents some criticalities related to the higher coolant temperature. The predicted pressure drop is within the limits, but thermal hot spots are observed in the CB, SL, and the passively-cooled supports, while potential local vaporisation issues are predicted by the analyses. Furthermore, coolant distribution in the RPs should be redefined to avoid fluid stagnation and flow reversal. These findings, resulting from the increased CB coolant operating temperature, suggest the need to revise the cassette structures and their cooling circuit design, with particular attention to the supports.

Additionally, the constraints on saturation margin and pressure drop considered for the CB cooling circuit should be updated, to adapt them to the revised operating conditions.

CRediT authorship contribution statement

F.M. Castrovinci: Writing – review & editing, Writing – original draft, Visualization, Investigation, Formal analysis, Conceptualization. **A. Quartararo:** Writing – review & editing, Writing – original draft, Visualization, Validation, Supervision, Methodology, Investigation, Formal analysis, Conceptualization. **S. Basile:** Writing – review & editing, Supervision, Funding acquisition. **G. Bongiovì:** Writing – review & editing, Supervision, Funding acquisition. **R. Burlon:** Writing – review & editing, Supervision, Funding acquisition. **P. Chiovaro:** Writing – review & editing, Supervision, Funding acquisition. **P.A. Di Maio:** Writing – review & editing, Supervision, Funding acquisition. **A. Gioè:** Writing – review & editing, Visualization, Investigation. **S. Maggio:** Writing – review & editing, Visualization, Investigation. **G. Mazzone:** Writing – review & editing, Project administration, Funding acquisition. **E. Tomarchio:** Writing – review & editing, Supervision, Funding acquisition. **S. Vacca:** Writing – review & editing, Visualization, Investigation. **E. Vallone:** Writing – review & editing, Supervision, Methodology, Funding acquisition. **J.-H. You:** Writing – review & editing, Project administration, Funding acquisition.

Declaration of competing interest

The authors declare that they have no known competing financial interests or personal relationships that could have appeared to influence the work reported in this paper.

Acknowledgements

This work has been carried out within the framework of the EUROfusion Consortium, funded by the European Union via the Euratom Research and Training Programme (Grant Agreement No 101052200 — EUROfusion). Views and opinions expressed are however those of the author(s) only and do not necessarily reflect those of the European Union or the European Commission. Neither the European Union nor the European Commission can be held responsible for them.

The computing resources and the related technical support used for this work have been provided by CRESCO/ENEAGRID High Performance Computing infrastructure and its staff [29]. CRESCO/ENEAGRID High Performance Computing infrastructure is funded by ENEA, the Italian National Agency for New Technologies, Energy and Sustainable Economic Development and by Italian and European research programmes, see [13] for information.

Data availability

Data will be made available on request.

References

[1] J.H. You, et al., Divertor of the European DEMO: Engineering and technologies for power exhaust, Fusion Eng. Des. 175 (2022) 113010, http://dx.doi.org/10.1016/j.fusengdes.2022.113010.
[2] G. Mazzone, et al., Choice of a low operating temperature for the DEMO EUROFER97 divertor cassette, Fusion Eng. Des. 124 (2017) 655–658, http://dx.doi.org/10.1016/j.fusengdes.2017.02.013.
[3] P.A. Di Maio, et al., Thermal-hydraulic study of the DEMO divertor cassette body cooling circuit equipped with a liner and two reflector plates, Fusion Eng. Des. 167 (2021) 112227, http://dx.doi.org/10.1016/j.fusengdes.2021.112227.
[4] D. Marzullo, et al., Selection of EU-DEMO divertor operating conditions: water cooling thermal-hydraulic parameters and power exhaust capabilities, Fusion Eng. Des. 203 (2024) 114467, http://dx.doi.org/10.1016/j.fusengdes.2024.114467.
[5] ANSYS Inc., ANSYS CFX-Solver Theory Guide, 2021, Release: 2021 R1.
[6] D. Marzullo, DIV-DEMO.S.1-T010-D001_DEMO Divertor CAD model 2022, 2023, EUROfusion IDM Ref.: 2Q43XL v1.0.
[7] P.A. Di Maio, et al., Hydraulic assessment of an upgraded pipework arrangement for the DEMO divertor plasma facing components cooling circuit, Fusion Eng. Des. 168 (2021) 112368, http://dx.doi.org/10.1016/j.fusengdes.2021.112368.
[8] A. Quartararo, et al., Thermofluid-dynamic assessment of the EU-DEMO divertor single-circuit cooling option, Fusion Eng. Des. 188 (2023) 113408, http://dx.doi.org/10.1016/j.fusengdes.2022.113408.
[9] J. Aktaa, et al., Embrittlement of WCLL blanket and its fracture mechanical assessment, Nucl. Fusion 63 (9) (2023) 096016, http://dx.doi.org/10.1088/1741-4326/ace984.
[10] P. Arena, et al., Design and Integration of the EU-DEMO Water-Cooled Lead Lithium Breeding Blanket, Energies 16 (4) (2023) 2069, http://dx.doi.org/10.3390/en16042069.
[11] I. Moscato, et al., Tokamak cooling systems and power conversion system options, Fusion Eng. Des. 178 (2022) 113093, http://dx.doi.org/10.1016/j.fusengdes.2022.113093.
[12] A. Quartararo, et al., Hypothetical porous medium concept as a virtual swirl tape: A novel modelling technique towards efficient CFD simulation of swirl tape cooling pipe, Fusion Eng. Des. 200 (2024) 114240, http://dx.doi.org/10.1016/j.fusengdes.2024.114240.
[13] http://www.cresco.enea.it/english.
[14] A. Quartararo, P. A. Di Maio, E. Vallone, ADRANOS: A numerical tool developed to analyse coolant operating conditions of the EU-DEMO divertor, Fusion Eng. Des. 197 (2023) 114055, http://dx.doi.org/10.1016/j.fusengdes.2023.114055.
[15] S. Vacca, et al., Thermal–hydraulic study of the Primary Heat Transport System of the EU-DEMO Divertor Plasma Facing Components, Fusion Eng. Des. 201 (2024) 114241, http://dx.doi.org/10.1016/j.fusengdes.2024.114241.
[16] R. Villari, S. Noce, M. Lungaroni, DIV-DEMO.S.1-T022-D001_Neutronics and shielding assessment report 2023, 2024, EUROfusion IDM Ref.: 2R7NAT v1.0.
[17] G. Mazzone, et al., Eurofusion-DEMO Divertor - Cassette Design and Integration, Fusion Eng. Des. 157 (2020) 111656, http://dx.doi.org/10.1016/j.fusengdes.2020.111656.
[18] A.R. Raffray, et al., Critical heat flux analysis and R&D for the design of the ITER divertor, Fusion Eng. Des. 45 (4) (1999) 377–407, http://dx.doi.org/10.1016/S0920-3796(99)00053-8.
[19] J. Mahaffy, et al., Best practice guidelines for the use of CFD in nuclear reactor safety applications, Tech. rep, Organisation for Economic Co-Operation and Development, 2007.
[20] International Association for the Properties of Water and Steam, Revised Release on the IAPWS Industrial Formulation 1997 for the Thermodynamic Properties of Water and Steam, 2007.
[21] F. Gillemot, et al., Material Property Handbook pilot project on EUROFER97 (MTA EK, KIT), 2016, EUROfusion IDM Ref.: 2MRP77.
[22] ITER Material Properties Handbook, ITER Document No. G74 MA 16.
[23] ITER SDC-IC Appendix A Materials Design Limit Data, 2013.
[24] E. Gaganidze, et al., DEMO-DEF-1-CD1 - Materials Properties Handbook - CuCrZr, 2020, EUROfusion IDM Ref.: 2NV3Q6.
[25] The American Society of Mechanical Engineers, Boiler and pressure vessel code, Section II - Part D, 2015.
[26] T. Haertl, et al., Rationale for the selection of the operating temperature of the DEMO vacuum vessel, Fusion Eng. Des. 146 (2019) 1096–1099, http://dx.doi.org/10.1016/j.fusengdes.2019.02.014.
[27] D.C. Groeneveld, et al., The 2006 CHF look-up table, Nucl. Eng. Des. 237 (15) (2007) 1909–1922, http://dx.doi.org/10.1016/j.nucengdes.2007.02.014.
[28] P.J. Linstrom, W.G. Mallard (Eds.), NIST Chemistry WebBook, in: NIST Standard Reference Database Number 69, National Institute of Standards and Technology, Gaithersburg MD, 20899, 2019, http://dx.doi.org/10.18434/T4D303, (retrieved September 9, 2019).
[29] F. Iannone, et al., CRESCO ENEA HPC clusters: a working example of a multifabric GPFS spectrum scale layout, in: 2019 International Conference on High Performance Computing Simulation, HPCS, 2019, pp. 1051–1052.